Acta Mechanica 186, 141–159 (2006)
DOI 10.1007/s00707-006-0343-6

Acta Mechanica
Printed in Austria

Slip effects on the peristaltic flow of a non-Newtonian Maxwellian fluid

E. F. El-Shehawy, **N. T. El-Dabe**, Cairo, and **I. M. El-Desoky**, Menofia, Egypt

Received September 12, 2005; revised January 3, 2006
Published online: July 26, 2006

Summary. In real systems there is always a certain amount of slip, which, however, is hard to detect experimentally because of the required space resolution. In this paper, we analyze the effect of slip boundary conditions on the dynamics of fluids in porous media by studying the flow of a Newtonian and non-Newtonian Maxwellian fluid in an axisymmetric cylindrical tube (pore), in which the flow is induced by traveling transversal waves on the tube wall. Like in peristaltic pumping, the traveling transversal waves induce a net flow of the liquid inside the pore. The viscosity as well as the compressibility of the liquid is taken into account. This problem has numerous applications in various branches of science, including stimulation of fluid flow in porous media under the effect of elastic waves and studies of blood flow dynamics in living creatures. The Navier-Stokes equations for an axisymmetric cylindrical pore are solved by means of a perturbation analysis, in which the ratio of the wave amplitude to the radius of the pore is small parameter. In the second order approximation, a net flow induced by the traveling wave is calculated for various values of the compressibility of the liquid, relaxation time and Knudsen number. The calculations disclose that the compressibility of the liquid, Knudsen number of slip flow and non-Newtonian effects in presence of peristaltic transport have a strong influence of the net flow rate. The effects of all parameters of the problem are numerically discussed and graphically explained.

1 Introduction

Investigation of flow dynamics of a fluid in a pore having circular cross section, induced by a wave traveling on its wall (boundary), has many applications in various branches of science. The physical mechanism of the flow induced by the traveling wave can be well understood and is known as the so-called peristaltic transport mechanism. This mechanism is a natural cause of motion of fluids in the body of living creatures and it frequently occurs in organs such as ureters, intestines, and arterioles. Peristaltic pumping is also used in medical instruments such as the heart-lung machine etc. [1].

The ''no slip'' boundary condition is widely used for flows involving non-Newtonian fluids past solid boundaries. However, it has been found that a large class of polymeric materials slip or stick-slip on solid boundaries. For instance, when polymeric melts flow due to an applied pressure gradient, there is a sudden increase in the throughput at a critical pressure gradient [2]. In real systems there is always a certain amount of slip, which, however, is hard to detect experimentally because of the required space resolution. No-slip boundary conditions are a convenient idealization of the behavior of viscous fluids near walls. The boundary conditions

relevant to flowing fluids are very important in predicting fluid flows in many applications. According to the findings of modern tribology, in the thin-film lubrication regime the thickness of the lubricating film reaches molecular dimensions and nanometer scales [3]. For these ultrathin films it is very difficult to determine the boundary conditions and fluid properties by experimental measurement. In these thin films the expected shear rates can be very high and beyond the values that can be studied in laboratories. Molecular-dynamics (MD) simulations, however, have proved to be an efficient method in investigating these complex systems at high shear rates and extreme conditions.

Kwang and Fang [4] studied the peristaltic transport in a slip flow in a two-dimensional channel in which the walls of the channel are imposed traveling sinusoidal waves of small amplitude. They found that there are velocity slips along both walls, the backward fluid flow is much more easily triggered than no-slip ones inside the channel so that the pumping power should be increased at the beginning. Georgios and Crochet [5] studied the compressible viscous flow in slits with slip at the wall. They studied the time-dependent compressible flow of a Newtonian fluid in slits using an arbitrary nonlinear slip law relating the shear to the velocity at the wall in absence of peristaltic motion. With the aim of modeling the oscillations observed in constant piston speed rheometers and other extruding devices, they also carried out computations for a compressible viscous fluid flowing through a channel with slip at the walls. In this computations the constitutive equation for slip was chosen to have a non-monotone relationship with the shear stress. By using a compressible fluid and a non-monotone constitutive equation for the slip, they were able to model the self-sustaining oscillations observed in the experiments. Recently, Lu et al. [6] studied the mechanical description of interfacial slips for quartz crystal micro balances with viscoelastic liquid loading, and found that an interfacial slip phenomenon is expected to occur at the interface between the surface of a quartz crystal sensor and the contacted liquid environment.

An experimental study of the dynamic response of a Newtonian fluid and a Maxwellian fluid under an oscillating pressure gradient was presented by Castrejon et al. [7] and Torretal et al. [8]. Laser Doppler anemometry (LDA) was used in order to determine the velocity of the fluid inside a cylindrical tube. They compared the previous theoretical work with their experimental LDA measurements. They used the non-slip condition to explain experiments of Maxwellian fluids flowing in tubes under oscillatory conditions. They found out that there is disagreement in the dynamic response between experimental values and the theoretical prediction. One of the possible causes of this disagreement in the response amplitude is because the fluid was locally under higher shear rates than its Maxwellian limit. The effect of the shear stress on the slip velocity was studied by Rao and Rajabol [9]. They studied the effect of slip boundary conditions on the flow of the fluids in a channel. They investigated the flow of a linearly viscous fluid when the slip depends on both the shear stress and the normal stress. If the shear stress at the wall is greater than the critical shear stress, the flow slips at the wall and conversely if the shear stress is not large enough, then the classical Poiseulle solution with no-slip is observed. Slip flow heat transfer in circular tubes was studied by Francisco et al. [10]. They showed that heat transfer depends on two parameters: the slip parameter (Knudsen number Kn), which is a measure of the degree of rarefaction, and on the surface accommodation coefficients. In the slip-flow regime, departure from continuum behavior is slight, corresponding to Knudsen numbers in the range of $10^{-3} - 10^{-1}$. Such a deviation from continuum behavior arises first from the walls, where in a non-negligible Knudsen layer molecular collisions with the walls dominate over inter-molecular collisions. Far from this layer intermolecular collisions are dominant. Hence, it is intuitive to model flow and heat transfer phenomena in slip flows by maintaining the usual continuum equations for the bulk of the fluid (Navier-Stokes, Fourier

heat conduction law) and relegating rarefaction effects to the boundary conditions for the temperature and velocity fields (thereby incorporating wall effects). Researchers Chu, W. K.-H and Chu, K.-H. W. [11], [12] have started to investigate the slip flow (which means the Knudsen number Kn in this flow regime satisfies $0.001 < \mathrm{Kn} < 0.15$; $\mathrm{Kn} = \mathrm{mfp/L}$, mfp is the mean free path of the gas, L is the characteristic length) within static, rigid, and corrugated-wall micro-channels or micro-tubes which are common in MEMS (Micro-Electro-Mechanical System) applications. The micro-domain will induce the slip flow because of the low-pressure environment or the characteristic length scale of cross-section being in microns. The non-zero velocity-slip at the walls normally comes from the incomplete momentum transfer along the gas-surface interacting (collision and reflection) boundary when the gas density in the channel is rather low [13].

In-vitro measurements in the context of blood flows, performed in micro-fabricated micro-channels are subjected to the channel walls exhibiting some degree of roughness. Interestingly it is realistic to note that micro-domains such as arteries and capillaries are prone to constrictions for various pathological reasons. Such micro-domain flow problems may be studied as flows through axially corrugated pipes using continuum theory, with slip boundary condition prescribed on the surface of the pipe. Though it is customary to treat fluid as a continuum medium in flow through micro domains, the validity of continuum approach depends on the value of the Knudsen number [14]. If $\mathrm{Kn} < 0.001$, so that the molecular mean free path of the molecules is negligible in comparison to the geometrical dimensions, the fluid can be treated as a continuous medium. If Kn lies between 0.001 and 0.1, it is found that the fluid loses grip on the boundaries and tends to slip among the walls of the domain, thereby producing an effect similar to that which would be caused by a reduction in viscosity. Still the continuum approach can hold, provided a suitable correction is made in the kinematical boundary conditions, allowing for fluidslip at the wall. Effect of the wall roughness on slip and rheological properties of the lubricant was studied in [3]. A sinusoidal wall model was used to study the effect of the size of asperities and their frequency on the wall slip. It was shown that as the period of roughness is increased, the degree of slip on the wall also increases. Also, they observed that with the larger roughness amplitudes it is possible to decrease the slip. It was also shown that with shorter molecules the amount of slip would be dramatically lower. Yingxi and Steve [15] studied the limits of the hydrodynamic no-slip boundary condition experimentally. Hydrodynamic forces were compared for the flow of Newtonian fluids past surfaces of variable roughness but similar, poorly wetted, surface chemistry. Their experiments show, for the first time to the best of our knowledge, how large the surface roughness must be to produce the no-slip boundary condition. There are potential implications in applications such as magnetic recording and microfluidics, where roughness can be designed to be very low.

With the above discussion in mind we note that there is disagreement in the dynamic response between experimental values and the theoretical prediction. One of the possible causes of this disagreement in the response amplitude is because the fluid was locally under higher shear rates than its Maxwellian limit. If the shear stress at the wall is greater than the critical shear stress, the flow slips at the wall, and conversely if the shear stress is not large enough, then the classical Poiseulle solution with no-slip is observed. So, the slip seems to be critical in determining the characteristics of the flow. Another importance of slip effects on Maxwellian fluids comes from the flow of blood in micro-channels as mentioned above. So, we suppose that it seems reasonable to investigate the effect of slip boundary conditions (assuming that the slip velocity depends on the shear stress only) on the dynamics of fluids in porous media by studying the flow of a Newtonian and Non-Newtonian Maxwell fluid in an axisymmetric cylindrical tube (pore), in which the flow is induced by traveling transversal waves on the tube

wall (peristaltic transport). This model may be applied to the movement of the chyme in the small intestine, by considering the chyme as a compressible liquid. The analysis is been carried out using a perturbation method in which the ratio of the wave amplitude to the radius of the pore is the small parameter. The net flow is obtained in explicit form. Moreover, the net flow induced by the traveling waves in presence of slip flow is calculated for various values of the compressibility number, relaxation time and Knudsen number. Actually we extend the analysis of Yin and Fung [16] by taking the slip effect at the wall into account. It is also an extension of the later work of Aarts and Ooms [1], in which the compressibility has been taken into account and of Tsiklauri and Bresenev [17], where the non-Newtonian effects have been incorporated.

2 Formulation of the problem

We consider an axisymmetric cylindrical tube (pore) of radius R and length L. We assume that an elastic wave induces a traveling wave on the wall (boundary) of the tube with the displacement of the form

$$W(z,t) = R + a\cos\left(\frac{2\pi}{\lambda}(z - ct)\right), \tag{1}$$

where a is the amplitude of the traveling wave, while λ and c are its wave length and velocity, respectively. We note that the z-axis of the (r,ϕ,z) cylindrical coordinate system is directed along the axis of the tube.

The equations that govern the flow are the balance of mass

$$\frac{\partial\rho}{\partial t} + \vec{\nabla}.(\rho\ \vec{v}) = 0 \tag{2}$$

and the momentum equation

$$\rho\frac{\partial\vec{v}}{\partial t} + \rho\,(\vec{v}.\vec{\nabla})\,\vec{v} = -\vec{\nabla}\,p\ -\ \vec{\nabla}\,\tilde{\tau}, \tag{3}$$

where ρ is the liquid density, p the pressure, $\vec{v}$ the velocity vector and $\tilde{\tau}$ represents the viscous stress tensor. We describe the viscoelastic properties of the fluid using Maxwell's model [18], which assumes that

$$t_m\frac{\partial\tilde{\tau}}{\partial t} = -\mu\vec{\nabla}\ \vec{v} - \frac{\mu}{3}\vec{\nabla}.\vec{v}\ -\ \tilde{\tau}, \tag{4}$$

where μ is the viscosity coefficient and t_m is the relaxation time.

We further assume that the equation of state [19]

$$\frac{1}{\rho}\frac{\partial\rho}{\partial p} = k^* \tag{5}$$

holds, where k^* is the compressibility of the liquid. The solution of this equation for the density as a function in the pressure is given by

$$\rho = \rho_0 e^{[k^*(p-p_0)]}, \tag{6}$$

where ρ_0 is the constant density at the reference pressure p_0.

The boundary conditions that must be satisfied by the fluid on the wall are the slip conditions. For the slip flow the fluid still obeys the Navier-Stokes equation, but the no-slip condition is replaced by the slip equation $u_t = A_p\,\partial u_t/\partial n$, where u_t is the tangential velocity, n is normal to the surface, and A_p is a coefficient close to mean free path of the molecules of the

fluid [20]. This condition has been attributed to Beavers and Joseph [21] for a porous boundary, but it was Navier who proposed it a century ago. Although the Navier condition looked simple, analytically it is much more difficult than the no-slip condition, then the boundary conditions on the wall are

$$v_r(W, z, t) = \frac{\partial W}{\partial t}, \quad v_z(W, z, t) = A\frac{\partial v_z}{\partial r}, \tag{7}$$

where A is the mean free path of the molecules of the liquid.

Equation (4) can be rewritten in the following form:

$$\left(1 + t_m \frac{\partial}{\partial t}\right)\tilde{\tau} = -\mu\vec{\nabla}\,\vec{v} - \frac{\mu}{3}\,\vec{\nabla}.\vec{v}. \tag{8}$$

Further, we apply the operator $\left(1 + t_m \frac{\partial}{\partial t}\right)$ to the momentum Eq. (3) and eliminate $\tilde{\tau}$ in it using Eq. (7):

$$\left(1 + t_m \frac{\partial}{\partial t}\right)\left(\rho\frac{\partial \vec{v}}{\partial t} + \rho(\vec{v}.\vec{\nabla})\vec{v}\right) = -\left(1 + t_m \frac{\partial}{\partial t}\right)\vec{\nabla}p + \mu\vec{\nabla}^2\,\vec{v} + \frac{\mu}{3}\,\vec{\nabla}(\vec{\nabla}.\vec{v}). \tag{9}$$

In cylindrical coordinates, the mass balance Eq. (2) reads

$$\frac{\partial \rho}{\partial t} + v_r\frac{\partial \rho}{\partial r} + v_z\frac{\partial \rho}{\partial z} + \rho\left(\frac{\partial v_r}{\partial r} + \frac{v_r}{r} + \frac{\partial v_z}{\partial z}\right) = 0, \tag{10}$$

while the Navier-Stokes Eq. (4) becomes

$$\left(1 + t_m \frac{\partial}{\partial t}\right)\left\{\rho\frac{\partial v_r}{\partial t} + \rho\left(v_r\frac{\partial v_r}{\partial r} + v_z\frac{\partial v_r}{\partial z}\right)\right\} = -\left(1 + t_m \frac{\partial}{\partial t}\right)\frac{\partial p}{\partial r}$$

$$+ \mu\left(\frac{\partial^2 v_r}{\partial r^2} + \frac{1}{r}\frac{\partial v_r}{\partial r} - \frac{v_r}{r^2} + \frac{\partial^2 v_r}{\partial z^2}\right) + \frac{\mu}{3}\frac{\partial}{\partial r}\left(\frac{\partial v_r}{\partial r} + \frac{v_r}{r} + \frac{\partial v_z}{\partial z}\right), \tag{11}$$

$$\left(1 + t_m \frac{\partial}{\partial t}\right)\left\{\rho\frac{\partial v_z}{\partial t} + \rho\left(v_r\frac{\partial v_z}{\partial r} + v_z\frac{\partial v_z}{\partial z}\right)\right\} = -\left(1 + t_m \frac{\partial}{\partial t}\right)\frac{\partial p}{\partial z}$$

$$+ \mu\left(\frac{\partial^2 v_z}{\partial r^2} + \frac{1}{r}\frac{\partial v_z}{\partial z} + \frac{\partial^2 v_z}{\partial z^2}\right) + \frac{\mu}{3}\frac{\partial}{\partial z}\left(\frac{\partial v_r}{\partial r} + \frac{v_r}{r} + \frac{\partial v_z}{\partial z}\right). \tag{12}$$

It would be expedient to simplify these equations by introducing non-dimensional variables. We have a characteristic velocity c and have characteristic lengths a, λ, and R. The following variables based on c and R could thus be introduced:

$$\overline{W} = \frac{W}{R}, \quad \overline{v_r} = \frac{v_r}{c}, \quad \overline{v_z} = \frac{v_z}{c}, \quad \overline{\rho} = \frac{\rho}{\rho_0}, \quad \overline{p} = \frac{p}{\rho_0 c^2}, \quad \overline{p_0} = \frac{p_0}{\rho_0 c^2}, \quad \overline{t} = \frac{ct}{R}.$$

The amplitude ratio ε, the wave number α, the Reynolds number Re, the Knudsen number Kn and the compressibility number χ are defined by

$$\varepsilon = \frac{a}{R}, \quad \alpha = \frac{2\pi R}{\lambda}, \quad \mathrm{Re} = \frac{\rho_0 cR}{\mu}, \quad \mathrm{Kn} = \frac{A}{R} \quad \text{and} \quad \chi = k^*\,\rho_0 c^2.$$

Under the above assumptions Eqs. (6) and (10)–(12) can be rewritten in the non-dimensional form after dropping the bars as

$$\frac{\partial \rho}{\partial t} + v_r\frac{\partial \rho}{\partial r} + v_z\frac{\partial \rho}{\partial z} + \rho\left(\frac{\partial v_r}{\partial r} + \frac{v_r}{r} + \frac{\partial v_z}{\partial z}\right) = 0, \tag{13}$$

$$\left(1+t_m\frac{\partial}{\partial t}\right)\left\{\rho\frac{\partial v_r}{\partial t}+\rho\left(v_r\frac{\partial v_r}{\partial r}+v_z\frac{\partial v_r}{\partial z}\right)\right\}=-\left(1+t_m\frac{\partial}{\partial t}\right)\frac{\partial p}{\partial r}$$
$$+\frac{1}{\mathrm{Re}}\left(\frac{\partial^2 v_r}{\partial r^2}+\frac{1}{r}\frac{\partial v_r}{\partial r}-\frac{v_r}{r^2}+\frac{\partial^2 v_r}{\partial z^2}\right)+\frac{1}{3\mathrm{Re}}\frac{\partial}{\partial r}\left(\frac{\partial v_r}{\partial r}+\frac{v_r}{r}+\frac{\partial v_z}{\partial z}\right), \tag{14}$$

$$\left(1+t_m\frac{\partial}{\partial t}\right)\left\{\rho\frac{\partial v_z}{\partial t}+\rho\left(v_r\frac{\partial v_z}{\partial r}+v_z\frac{\partial v_z}{\partial z}\right)\right\}=-\left(1+t_m\frac{\partial}{\partial t}\right)\frac{\partial p}{\partial z}$$
$$+\frac{1}{\mathrm{Re}}\left(\frac{\partial^2 v_z}{\partial r^2}+\frac{1}{r}\frac{\partial v_z}{\partial z}+\frac{\partial^2 v_z}{\partial z^2}\right)+\frac{1}{3\mathrm{Re}}\frac{\partial}{\partial z}\left(\frac{\partial v_r}{\partial r}+\frac{v_r}{r}+\frac{\partial v_z}{\partial z}\right), \tag{15}$$

$$\rho=e^{\chi(p-p_0)}, \tag{16}$$

also the boundary conditions (7) become

$$v_r((1+\eta),z,t)=\frac{\partial\eta(z,t)}{\partial t},\quad v_z((1+\eta),z,t)=\mathrm{Kn}\frac{\partial v_z(r,z,t)}{\partial r}, \tag{17}$$

where

$$\eta(z,t)=\varepsilon\cos\alpha(z-t). \tag{18}$$

3 Method of solution

To illustrate the nature of the solution we shall consider the important case of no flow in absence of the peristaltic wave. Following [1], we seek the solution of the governing equations in a form

$$\begin{aligned}
&p=p_0+\varepsilon p_1(r,z,t)+\varepsilon^2 p_2(r,z,t)+\ldots,\\
&v_r=\varepsilon u_1(r,z,t)+\varepsilon^2 u_2(r,z,t)+\ldots,\\
&v_z=\varepsilon v_1(r,z,t)+\varepsilon^2 v_2(r,z,t)+\ldots,\\
&\rho=1+\varepsilon\rho_1(r,z,t)+\varepsilon^2\rho_2(r,z,t)+\ldots.
\end{aligned} \tag{19}$$

Then, doing a usual perturbation analysis using the latter expansions, we can obtain a closed set of governing equations for the first (ε) and second (ε^2) order as the following:

$$\left(1+t_m\frac{\partial}{\partial t}\right)\frac{\partial u_1}{\partial t}=-\left(1+t_m\frac{\partial}{\partial t}\right)\frac{\partial p_1}{\partial r}$$
$$+\frac{1}{\mathrm{Re}}\left(\frac{\partial^2 u_1}{\partial r^2}+\frac{1}{r}\frac{\partial u_1}{\partial r}-\frac{u_1}{r^2}+\frac{\partial^2 u_1}{\partial z^2}\right)+\frac{1}{3\mathrm{Re}}\frac{\partial}{\partial r}\left(\frac{\partial u_1}{\partial r}+\frac{u_1}{r}+\frac{\partial v_1}{\partial z}\right),$$
$$\left(1+t_m\frac{\partial}{\partial t}\right)\frac{\partial v_1}{\partial t}=-\left(1+t_m\frac{\partial}{\partial t}\right)\frac{\partial p_1}{\partial z}$$
$$+\frac{1}{\mathrm{Re}}\left(\frac{\partial^2 v_1}{\partial r^2}+\frac{1}{r}\frac{\partial v_1}{\partial r}+\frac{\partial^2 v_1}{\partial z^2}\right)+\frac{1}{3\mathrm{Re}}\frac{\partial}{\partial z}\left(\frac{\partial u_1}{\partial r}+\frac{u_1}{r}+\frac{\partial v_1}{\partial z}\right), \tag{20}$$
$$\frac{\partial\rho_1}{\partial t}+\frac{\partial u_1}{\partial r}+\frac{u_1}{r}+\frac{\partial v_1}{\partial z}=0,$$
$$\rho_1=\chi p_1,$$

$$
\begin{aligned}
&\left(1 + t_m \frac{\partial}{\partial t}\right)\left\{\frac{\partial u_2}{\partial t} + \rho_1 \frac{\partial u_1}{\partial t} + u_1 \frac{\partial u_1}{\partial r} + v_1 \frac{\partial u_1}{\partial z}\right\} = -\left(1 + t_m \frac{\partial}{\partial t}\right)\frac{\partial p_2}{\partial r} \\
&\quad + \frac{1}{\mathrm{Re}}\left(\frac{\partial^2 u_2}{\partial r^2} + \frac{1}{r}\frac{\partial u_2}{\partial r} - \frac{u_2}{r^2} + \frac{\partial^2 u_2}{\partial z^2}\right) + \frac{1}{3\mathrm{Re}}\frac{\partial}{\partial r}\left(\frac{\partial u_2}{\partial r} + \frac{u_2}{r} + \frac{\partial v_2}{\partial z}\right), \\
&\left(1 + t_m \frac{\partial}{\partial t}\right)\left\{\frac{\partial v_2}{\partial t} + \rho_1 \frac{\partial v_1}{\partial t} + u_1 \frac{\partial v_1}{\partial r} + v_1 \frac{\partial v_1}{\partial z}\right\} = -\left(1 + t_m \frac{\partial}{\partial t}\right)\frac{\partial p_2}{\partial z} \\
&\quad + \frac{1}{\mathrm{Re}}\left(\frac{\partial^2 v_2}{\partial r^2} + \frac{1}{r}\frac{\partial v_2}{\partial r} + \frac{\partial^2 v_2}{\partial z^2}\right) + \frac{1}{3\mathrm{Re}}\frac{\partial}{\partial z}\left(\frac{\partial u_2}{\partial r} + \frac{u_2}{r} + \frac{\partial v_2}{\partial z}\right), \\
&\frac{\partial \rho_2}{\partial t} + u_1 \frac{\partial \rho_1}{\partial r} + v_1 \frac{\partial \rho_1}{\partial z} + \frac{u_2}{r} + \frac{\partial u_2}{\partial r} + \frac{\partial v_2}{\partial z} + \rho_1\left(\frac{\partial u_1}{\partial r} + \frac{u_1}{r} + \frac{\partial v_1}{\partial z}\right) = 0, \\
&\rho_2 = \chi p_2 + \frac{1}{2}\chi^2 p_1^2.
\end{aligned}
\tag{21}
$$

Expanding Eq. (17) by Taylor expansion around $r = 1$ and substituting from Eq. (19) we get the following boundary conditions:

$$
\begin{aligned}
&u_1(1, z, t) = -\frac{i\alpha}{2}\left(e^{i\alpha(z-t)} - e^{-i\alpha(z-t)}\right), \\
&u_2(1,z,t) + \frac{1}{2}\left(e^{i\alpha(z-t)} + e^{-i\alpha(z-t)}\right)\frac{\partial u_1}{\partial r}(1,z,t) = 0, \\
&v_1(1,z,t) = \mathrm{Kn}\frac{\partial v_1}{\partial r}(1,z,t), \\
&v_2(1,z,t) + \frac{1}{2}\left(e^{i\alpha(z-t)} + e^{-i\alpha(z-t)}\right)\frac{\partial v_1}{\partial r}(1,z,t) \\
&\quad = \mathrm{Kn}\left[\frac{\partial v_2}{\partial r}(1,z,t) + \frac{1}{2}\left(e^{i\alpha(z-t)} + e^{-i\alpha(z-t)}\right)\frac{\partial^2 v_1}{\partial r^2}(1,z,t)\right].
\end{aligned}
\tag{22}
$$

Further, following [1] and [17], we seek the solution of the linear problem in the form

$$
\begin{aligned}
u_1(r,z,t) &= U_1(r)\, e^{i\alpha(z-t)} + \overline{U_1}(r)\, e^{-i\alpha(z-t)}, \\
v_1(r,z,t) &= V_1(r)\, e^{i\alpha(z-t)} + \overline{V_1}(r)\, e^{-i\alpha(z-t)}, \\
p_1(r,z,t) &= P_1(r)\, e^{i\alpha(z-t)} + \overline{P_1}(r)\, e^{-i\alpha(z-t)}, \\
\rho_1(r,z,t) &= \chi P_1(r)\, e^{i\alpha(z-t)} + \chi\, \overline{P_1}(r)\, e^{-i\alpha(z-t)}.
\end{aligned}
\tag{23}
$$

Here and in the following equations, the bar denotes a complex conjugate.

On the other hand, we seek the second (ε^2) order solution in the form

$$
\begin{aligned}
u_2(r,z,t) &= U_{20}(r) + U_2(r)\, e^{2i\alpha(z-t)} + \overline{U_2}(r)\, e^{-2i\alpha(z-t)}, \\
v_2(r,z,t) &= V_{20}(r) + V_2(r)\, e^{2i\alpha(z-t)} + \overline{V_1}(r)\, e^{-2i\alpha(z-t)}, \\
p_2(r,z,t) &= P_{20}(r) + P_2(r)\, e^{2i\alpha(z-t)} + \overline{P_2}(r)\, e^{-2i\alpha(z-t)}, \\
\rho_2(r,z,t) &= D_{20}(r) + D_2(r)\, e^{2i\alpha(z-t)} + \overline{D_2}(r)\, e^{-2i\alpha(z-t)}.
\end{aligned}
\tag{24}
$$

The latter choice of solution is motivated by the fact that the peristaltic flow is essentially a nonlinear (second-order) effect [1], and adding a nonoscillatory term in the first order gives only a trivial solution. Thus, we can add nonoscillatory terms, such as $U_{20}(r)$, $V_{20}(r)$, $P_{20}(r)$, and

$D_{20}(r)$, which do not cancel out in the solution after time averaging over the period, only in the second and higher orders.

Substituting from Eq. (23) into Eqs. (20) and (22) we obtain the following system of equations:

$$-i\alpha(1 - i\alpha t_m)U_1 = -(1 - i\alpha t_m)P_1' + \frac{1}{\mathrm{Re}}\left(U_1'' + \frac{U_1'}{r} - \frac{U_1}{r^2} - \alpha^2 U_1\right) + \frac{1}{3\mathrm{Re}}\frac{d}{dr}\left(U_1' + \frac{U_1}{r} + i\alpha V_1\right), \tag{25.1}$$

$$-i\alpha(1 - i\alpha t_m)V_1 = -i\alpha(1 - i\alpha t_m)P_1 + \frac{1}{\mathrm{Re}}\left(V_1'' + \frac{V_1'}{r} - \alpha^2 V_1\right) + \frac{i\alpha}{3\,\mathrm{Re}}\left(U_1' + \frac{U_1}{r} + i\alpha V_1\right), \tag{25.2}$$

$$U_1' + \frac{U_1}{r} + i\alpha V_1 = i\alpha\chi P_1, \tag{25.3}$$

$$U_1(1) = -\frac{i\alpha}{2}, \tag{25.4}$$

$$V_1(1) = \mathrm{Kn}\ V_1'(1). \tag{25.5}$$

Here, the prime denotes a derivative with respect to r.

Further, we rewrite the system of Eqs. (25.1–3) in the form

$$-\gamma P_1' + \left(U_1'' + \frac{U_1'}{r} - \frac{U_1}{r^2} - \beta^2 U_1\right) = 0, \tag{26.1}$$

$$-\gamma P_1 - \frac{i}{\alpha}\left(V_1 + \frac{V_1'}{r} - \beta^2 V_1\right) = 0, \tag{26.2}$$

where the complex parameters γ and β are given by

$$\gamma = (1 - i\alpha t_m)\mathrm{Re} - \frac{i\alpha\chi}{3}, \quad \beta^2 = \alpha^2 - i\alpha(1 - i\alpha t_m)\mathrm{Re}. \tag{27}$$

Eliminating $V_1(r)$ by using Eq. (25.3), we rewrite Eq. (26.2) as

$$-\frac{i\chi}{\alpha}\left[P_1'' + \frac{P_1'}{r} - \left(\beta^2 + \frac{i\alpha\gamma}{\chi}\right)P_1\right] + \frac{1}{\alpha^2}\left(\frac{d}{dr} + \frac{1}{r}\right)\left[U_1'' + \frac{U_1'}{r} - \frac{U_1}{r^2} - \beta^2 U_1\right] = 0. \tag{28}$$

Differentiating Eq. (28) with respect to r and using Eq. (26.1), we are led to the following equation:

$$-\frac{i\chi}{\alpha\gamma}\left(\frac{d^2}{dr^2} + \frac{1}{r}\frac{d}{dr} - \frac{1}{r_2} - \left(\beta^2 + \frac{i\alpha\gamma}{\chi}\right)\right)\left[U_1'' + \frac{U_1'}{r} - \frac{U_1}{r^2} - \beta^2 U_1\right] + \frac{1}{\alpha^2}\left(\frac{d^2}{dr^2} + \frac{d}{dr} - \frac{1}{r^2}\right)\left[U_1'' + \frac{U_1'}{r} - \frac{U_1}{r^2} - \beta^2 U_1\right] = 0. \tag{29}$$

This equation is rewritten, after multiplication by α^2, as

$$\left(1 - \frac{i\chi\alpha}{\gamma}\right)\left(\frac{d^2}{dr^2} + \frac{1}{r}\frac{d}{dr} - \frac{1}{r_2} - \upsilon^2\right)\left(\frac{d^2}{dr^2} + \frac{d}{dr} - \frac{1}{r^2} - \beta^2\right)U_1 = 0. \tag{30}$$

From this equation Eq. (30) we obtain the master equation for $U_1(r)$ and find its general solution as

$$U_1(r) = C_1 I_1(\upsilon r) + C_2 I_1(\beta r), \tag{31}$$

where I_1 is the modified Bessel function of the first kind of order 1. Note, that Eq. (31) is similar to Eq. (3.18) in [1], except that C_1 and C_2 are complex constants calculated using Eqs. (25.4–5) and defined by

$$\begin{aligned} C_1 &= \frac{i\alpha\beta\upsilon\,(I_0(\beta) - \beta\,\mathrm{Kn}\,I_1(\beta))}{2\left[\alpha^2 I_1(\beta) I_0(\upsilon) - \beta\upsilon I_1(\upsilon) I_0(\beta) + \upsilon\,\mathrm{Kn}\,I_1(\upsilon) I_1(\beta)\left(\beta^2 - \alpha^2\right)\right]}, \\ C_2 &= \frac{-i\alpha^3[I_0(\upsilon) - \upsilon\,\mathrm{Kn}\,I_1(\upsilon)]}{2\left[\alpha^2 I_1(\beta) I_0(\upsilon) - \beta\upsilon I_1(\upsilon) I_0(\beta) + \upsilon\,\mathrm{Kn}\,I_1(\upsilon) I_1(\beta)\left(\beta^2 - \alpha^2\right)\right]}, \end{aligned} \tag{32}$$

where

$$\upsilon^2 = \alpha^2 \frac{(1-\chi)\,(1 - i\alpha t_m)\mathrm{Re} - (4/3) i\alpha\chi}{(1 - i\alpha t_m)\,\mathrm{Re} - (4/3) i\alpha\chi}. \tag{33}$$

Here, I_0 is the modified Bessel function of the first kind of order 0.

We also obtain the general solution for $V_1(r)$:

$$V_1(r) = \frac{i\alpha C_1}{\upsilon} I_0(\upsilon r) + \frac{i\beta C_2}{\alpha} I_0(\beta r), \tag{34}$$

and the general solution for $P_1(r)$:

$$P_1(r) = \frac{C_1(\upsilon^2 - \beta^2)}{\gamma\upsilon} I_0(\upsilon r). \tag{35}$$

To solve the system of second order of ε, using Eq. (30) in Eqs. (27) and (28) we obtain the following set of equations:

$$D_{20} = \chi P_{20} + \chi^2 P_1 \overline{P_1}, \tag{36.1}$$

$$U_{20}' + \frac{U_{20}}{r} = -\chi\left(P_1\overline{U_1'} + \overline{P_1}U_1' + \frac{P_1\overline{U_1}}{r} + \frac{\overline{P_1}U_1}{r} + U_1\overline{P_1'} + \overline{U_1}P_1'\right), \tag{36.2}$$

$$\begin{aligned} &i\alpha\chi\, P_1\overline{U_1} - i\alpha\chi\overline{P_1}U_1 + U_1\overline{U_1'} + \overline{U_1}U_1' + i\alpha U_1\overline{V_1} - i\alpha\overline{U_1}V_1 \\ &\quad = -P_{20}' + \frac{1}{(1 - i\alpha t_m)\,\mathrm{Re}}\left(U_{20}'' + \frac{U_{20}'}{r} - \frac{U_{20}}{r^2}\right) + \frac{1}{3(1 - i\alpha t_m)\,\mathrm{Re}}\frac{d}{dr}\left(U_{20}' + \frac{U_{20}}{r}\right), \end{aligned} \tag{36.3}$$

$$i\alpha\chi P_1\overline{V_1} - i\alpha\chi\overline{P_1}V_1 + U_1\overline{V_1'} + \overline{U_1}V_1' = \frac{1}{(1 - i\alpha t_m)\mathrm{Re}}\left(V_{20}'' + \frac{V_{20}'}{r}\right), \tag{36.4}$$

$$U_{20}(1) + \frac{1}{2}\left(\overline{U_1'}(1) + U_1'(1)\right) = 0, \tag{36.5}$$

$$V_{20}(1) + \frac{1}{2}\left(\overline{V_1'}(1) + V_1'(1)\right) = \mathrm{Kn}\left(V_{20}'(1) + \frac{1}{2}V_1''(1) + \frac{1}{2}\overline{V_1''}(1)\right). \tag{36.6}$$

It will be seen that, as far as the net flow is considered, only the functions U_{20}, V_{20}, P_{20} and D_{20} contribute to the net flow as long as terms up to $O(\varepsilon^2)$ are retained. Thus, the functions U_2, V_2, P_2 and D_2 don't contribute to the net flow, and therefore we shall not write down the equations that these functions satisfy or solve them. We continue with the

solutions for U_{20}, V_{20}, P_{20} and D_{20} [1]. To that end, the second-order solution $U_{20}(r)$ can also be found in a way similar to the one used in the first order as follows:

$$U_{20}(r) = \frac{D_1}{r} - \chi\left[P_1(r)\,\overline{U_1}(r) + \overline{P_1}(r)\,U_1(r)\right], \tag{37}$$

where D_1 is a complex constant (which follows from the boundary conditions (36.4,5)) defined by $D_1 = \frac{i\,\alpha\,\mathrm{Kn}}{2}\left(V_1'(1) - \overline{V_1'}(1)\right)$, having the final form

$$D_1 = \frac{i\,\alpha\,\mathrm{Kn}}{2}\left(i\,\alpha\,C_1\,I_1(\upsilon) + \tfrac{i\,\beta^2\,C_2}{\alpha}I_1(\beta) + i\,\alpha\,\overline{C_1}\,I_1(\overline{\upsilon}) + \tfrac{i\,\overline{\beta}^2\,\overline{C_2}}{\alpha}I_1(\overline{\beta})\right). \tag{38}$$

We also obtain the general solution for $V_{20}(r)$ as follows:

$$V_{20}(r) = D_2 - (1 - i\,\alpha\,t_m)\mathrm{Re}\int_r^1 \left[V_1(\zeta)\,\overline{U_1}(\zeta) + \overline{V_1}(\zeta)\,U_1(\zeta)\right]d\zeta, \tag{39}$$

where D_2 is a complex constant defined by

$$D_2 = \frac{-1}{2}\left(V_1'(1) + \overline{V_1'}(1)\right) + \mathrm{Kn}\left(V_{20}'(1) + \frac{1}{2}V_1''(1) + \overline{V_1''}(1)\right), \tag{40}$$

where the values of $V_{20}'(1)$ and $V_1''(1)$ are defined by

$$\begin{aligned} V_{20}'(1) = (1 - i\,\alpha\,t_m)\mathrm{Re}\Bigg[&\frac{i\,\alpha\,C_1\,\overline{C_1}}{\upsilon}I_0(\upsilon)\,I_1(\overline{\upsilon}) + \frac{i\,\alpha\,C_1\,\overline{C_2}}{\upsilon}I_0(\upsilon)\,I_1(\overline{\beta}) \\ &+ \frac{i\,\beta\,C_2\,\overline{C_1}}{\alpha}I_0(\beta)\,I_1(\overline{\upsilon}) + \frac{i\,\beta\,C_2\,\overline{C_2}}{\alpha}I_0(\beta)\,I_1(\overline{\beta}) \\ &- \frac{i\,\alpha\,C_1\,\overline{C_1}}{\overline{\upsilon}}I_0(\overline{\upsilon})\,I_1(\upsilon) - \frac{i\,\alpha\,C_2\,\overline{C_1}}{\overline{\upsilon}}I_0(\overline{\upsilon})\,I_1(\beta) \\ &- \frac{i\,\overline{\beta}\,C_1\,\overline{C_2}}{\alpha}I_0(\overline{\beta})\,I_1(\upsilon) - \frac{i\,\overline{\beta}\,C_2\,\overline{C_2}}{\alpha}I_0(\overline{\beta})\,I_1(\beta)\Bigg], \end{aligned} \tag{41}$$

$$V_1''(1) = i\,\alpha\,C_1[\upsilon I_0(\upsilon) - I_1(\upsilon)] + \frac{i\,\beta^2 C_2}{\alpha}[\beta I_0(\beta) - I_1(\beta)]. \tag{42}$$

The dimensionless fluid flow rate Q can be calculated as [1]

$$Q(z,t) = 2\pi\left[\varepsilon\int_0^1 v_1(r,z,t)rdr + \varepsilon^2\int_0^1 v_2(r,z,t)rdr + O(\varepsilon^3)\right].$$

Next, the net flow is considered over one period of time. The average of a variable G over one period T of time t is

$$\langle G\rangle = \frac{1}{T}\int_0^T G(r,z,t)dt. \tag{43}$$

At $T = \frac{2\pi}{\alpha}$, consequently the mean net axial velocity $\langle V_z\rangle$ reads

$$\langle V_z\rangle = \varepsilon^2 V_{20}(r) \tag{44}$$

under neglect of $O(\varepsilon^3)$-terms, while the net flow rate $\langle Q\rangle$ is given by

$$\langle Q \rangle = 2\,\pi\,\varepsilon^2 \int_0^1 V_{20}(r)\, r\, dr \tag{45}$$

under neglect of $O(\varepsilon^3)$-terms. Thus, the traveling wave induces a net flow of the liquid, of which the (dimensionless) rate is expressed by Eq. (45). Hence, the net flow and the mean net axial velocity are an effect of order ε^2.

4 Numerical results and discussion

To study the behavior of the net flow rate, numerical calculations for several values of α, Kn, t_m and χ are carried out. We concentrate on the solution of the dimensionless problem as described in the previous section. It is clear that we have to choose $\varepsilon \ll 1$ because we used the perturbation method with the amplitude ratio ε as a parameter [22]. Also, for the perturbation method to be valid and accurate we must have $\varepsilon\,\alpha^2\ \mathrm{Re} << 1$ according to Takabatake [23].

We consider the net flow rate $\langle Q \rangle$ given by Eq. (45). After one integration by parts, $\langle Q \rangle$ can be expressed as

$$\langle Q \rangle = \pi\,\varepsilon^2 \left(D_2 - (1 - i\,\alpha\, t_m)\, Re \int_0^1 r^2 \left[V_1(r)\, \overline{U_1}(r) + \overline{V_1}(r)\, U_1(r) \right] dr \right), \tag{46}$$

where the solution of Eq. (39) for $V_{20}(r)$ is used.

A numerical code has been written to calculate $\langle Q \rangle$ according to Eq. (46). In order to check the validity of our code, we run it for the parameters similar to the ones used by other authors. For instance, for $\varepsilon = 0.15$, $\mathrm{Re} = 10000.0$, $\alpha = 0.20$, $\chi = 0.0$, $t_m = 0.0$ and $\mathrm{Kn} = 0.0$ we obtain $\langle Q \rangle = 0.2709$, which is equal (if we keep four digits after the decimal point) to the result of the authors of [16], who actually obtained $\langle Q \rangle = 0.2709$. Further, we have made several runs of our code for different values of the parameter Kn at $t_m = 0$ (Newtonian regime). We note again that Kn and t_m enter the equations because we have included the slip effects into the non-Newtonian Maxwell model. Eq. (46) will be identical to the similar equation (4.1) of [1] if we set $\mathrm{Kn} = 0.0$ and $t_m = 0.0$ in all our equations. Further, Eq. (46) will be identical to the similar equation (16) of [17] if we set $\mathrm{Kn} = 0.0$ in all our equations.

First, we investigate the effect of slip boundary conditions in the case of a Newtonian ($t_m = 0.0$) Maxwellian fluid. The results of our calculations are presented in Fig. 1, where we investigate the dependence of $\langle Q \rangle$ on the compressibility parameter χ for various values of Kn. In order to compare our results with the ones from [1], we have plotted $\langle Q \rangle$ for the following set of parameters: $\varepsilon = 0.001$, $\mathrm{Re} = 10000.0$, $\alpha = 0.001$, $t_m = 0.0$ and $\mathrm{Kn} = 0.0$. We note that the curve is identical to the corresponding curve (solid curve) in Fig. 2 from [1]. This obviously corroborates the validity of our numerical code. Further, to investigate the dependence of the flow rate $\langle Q \rangle$ on Kn we perform the calculation for a few values of Kn. We notice that the range of $\langle Q \rangle$ is approximately $0.4272 - 2.7043 \times 10^{-5}$ for the range of χ from 0 to 1. In particular, for $\chi = 0.0$ the range of $\langle Q \rangle$ is just $1.2305 - 1.4714 \times 10^{-5}$ for the three values of Kn considered, while for $\chi > 0$ the range becomes $0.0034 - 3.8223 \times 10^{-5}$. Hence, $\langle Q \rangle$ is weakly affected by Kn at $\chi = 0.0$. For $\chi > 0$ however, $\langle Q \rangle$ strongly depends on the Knudsen number of slip flow. Furthermore, we observe that for $\mathrm{Kn} = 0.0$ $\langle Q \rangle$ attains a maximum of 2.7141×10^{-5} at $\chi = 0.5$, and for $\chi > 0.5$ the flow rate decreases to 0.4901×10^{-5}, while for $\mathrm{Kn} = 0.05$ $\langle Q \rangle$ attains a maximum of 2.9734×10^{-5} at $\chi = 0.4$ and for $\chi > 0.4$ the flow rate decreases until it

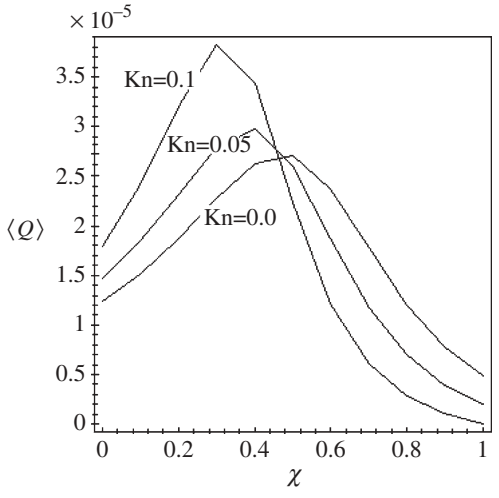

Fig. 1. The dimension less flow rate $\langle Q \rangle$ versus χ at $\varepsilon = 0.001$, $\mathrm{Re} = 10000.0$, $t_m = 0.0$ and $\alpha = 0.001$

reaches 0.2075×10^{-5}; for $\mathrm{Kn} = 0.1$ $\langle Q \rangle$ attains a maximum of 3.8226×10^{-5} at $\chi = 0.3$ and for $\chi > 0.3$ the flow rate decreases until it reaches 0.0035×10^{-5}. Thus, we note that at high values of Kn the rate of decreasing of $\langle Q \rangle$ is greater than at low values. Furthermore, the compressibility number χ has a significant influence on the net flow rate, and the Knudsen number Kn plays a more significant role in the net flow of a compressible liquid than of an incompressible one.

In Fig. 2 we investigate the behavior of the net flow rate $\langle Q \rangle$ depending on the parameter α, which is the tube radius measured in wavelengths. Again, to check for the consistency of our numerical results with the ones of [1], and also to investigate phenomena brought about by the introduction of slip effects into the model (non-Newtonian Maxwell fluid), we plot the net flow rate $\langle Q \rangle$ versus α for the following set of parameters: $\varepsilon = 0.001$, $\mathrm{Re} = 10000.0$, $\chi = 0.6$, $t_m = 0.0$ and $\mathrm{Kn} = 0.0$. If we compare this curve in our Fig. 2 with the dashed curve in Fig. 3 of [1], we will note no difference, which again corroborates the validity of our numerical code. We then set Kn to various nonzero values and investigate the changes induced by slip effects. We note that the net flow rate $\langle Q \rangle$ attains a maximum for a certain value of α, and this maximum

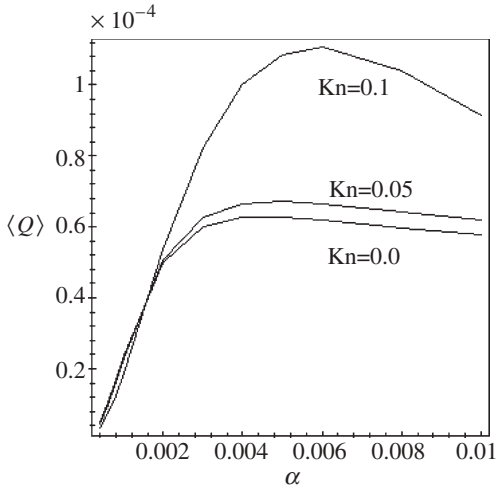

Fig. 2. The dimensionless flow rate $\langle Q \rangle$ versus α at $\varepsilon = 0.001$, $\mathrm{Re} = 10000.0$, $t_m = 0.0$ and $\chi = 0.6$

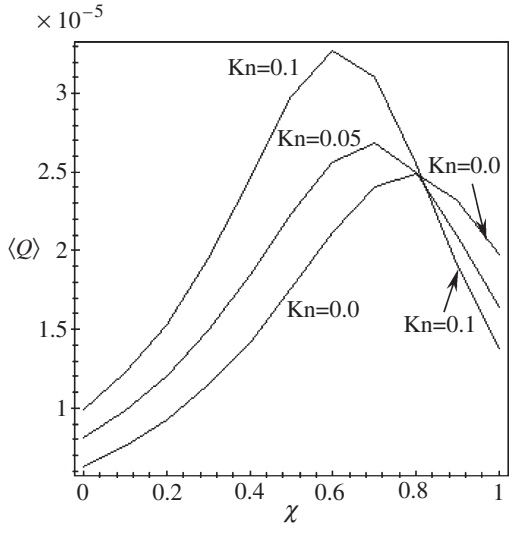

Fig. 3. The dimensionless net flow rate $\langle Q \rangle$ versus χ at $\varepsilon = 0.001$, $\mathrm{Re} = 10000$, $t_m = 1000$ and $\alpha = 0.001$

increases with increasing Kn. Furthermore, after $\langle Q \rangle$ reaches the maximum value it then decreases with increasing α, but this decreasing is greatest at high values of Kn. Also we can note that $\langle Q \rangle$ is nearly independent of Kn for $\alpha < 0.001$.

Second, we investigate the effect of slip boundary conditions in the case of a non-Newtonian Maxwellian fluid. It is known that viscoelastic fluids, described by the Maxwellian fluid, have different flow regimes depending on the value of the parameter $\mathrm{De} = t_v/t_m$, which is called the Deborah number. In effect, the Deborah number is a ratio of the characteristic time of viscous effects $t_v = \rho R^2/\mu$ to the relaxation time t_m. As noted in [18], the value of the parameter De (which the authors of [18] actually call α) determines in which regime the system resides. Beyond a certain critical value ($\mathrm{De} = 11.64$), the system is dissipative and conventional viscous effects dominate. On the other hand, for small De ($\mathrm{De} < \mathrm{De}_c$) the system exhibits viscoelastic behavior.

The results of our calculations are presented in Fig. 3, where we investigate the dependence of $\langle Q \rangle$ on the compressibility parameter χ for various values of Kn. In order to compare our results with the ones from [17], we have plotted $\langle Q \rangle$ for the following set of parameters: $\varepsilon = 0.001$, $\mathrm{Re} = 10000.0$, $\alpha = 0.001$, $t_m = 1000$ and $\mathrm{Kn} = 0.0$. We note that the curve is identical to the corresponding curve in Fig. 1 (dashed-dotted curve with asterisks) from [17]. This obviously corroborates the validity of our numerical code. Further, to investigate the dependence of the flow rate $\langle Q \rangle$ on Kn, we perform the calculation for a few values of Kn. When $\mathrm{Kn} = 0.0$ we observe that the net flow rate reaches a maximum value $\langle Q \rangle = 2.4918 \times 10^{-5}$ at $\chi = 0.8$. Further, when Kn=0.05 we notice that the maximum value $\langle Q \rangle = 2.6858 \times 10^{-5}$ at $\chi = 0.7$. The maximum value of $\langle Q \rangle = 3.2682 \times 10^{-5}$ and occurs at $\chi = 0.6$ when $\mathrm{Kn} = 0.1$. From the above discussion, we notice that $\langle Q \rangle$ attains a maximum for a certain value of χ and this maximum increases with increasing Kn. Moreover, there is shifting the maximum value of $\langle Q \rangle$ towards lower values of χ's with increasing Kn.

In Fig. 4 we investigate the behavior of the flow rate $\langle Q \rangle$ depending on the compressibility parameter χ at $t_m = 10000$ (deeply non-Newtonian regime). Again, to check for the consistency of our numerical results with the ones of [16], we first plot $\langle Q \rangle$ versus χ for the following set of parameters: $\varepsilon = 0.001$, $\mathrm{Re} = 10000.0$, $\alpha = 0.001$ and $\mathrm{Kn} = 0.0$. If we compare the curve in our Fig. 4 with the dashed curve with empty squares in Fig. 1 from [17], we will note no difference,

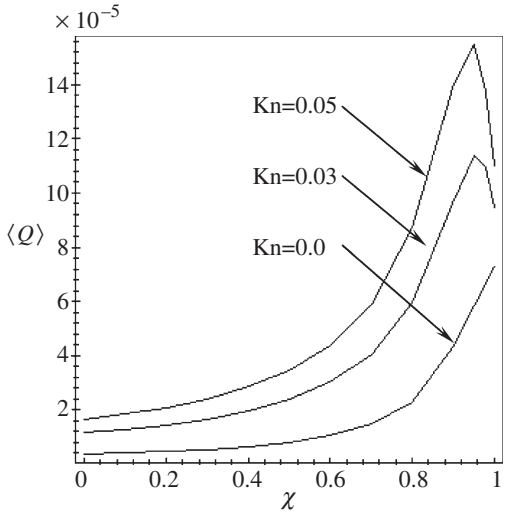

Fig. 4. The dimensionless net flow rate $\langle Q \rangle$ versus χ at $\varepsilon = 0.001$, $\mathrm{Re} = 10000$, $t_m = 10000$ and $\alpha = 0.001$

which again corroborates the validity of our numerical code. We then set Kn to various nonzero values and investigate the effect of Kn at deeply non-Newtonian regime. In this deeply non-Newtonian regime we notice that when $\mathrm{Kn} = 0.0$ the maximum value of $\langle Q \rangle = 7.2545 \times 10^{-5}$ at $\chi = 1.0$,whereas when $\mathrm{Kn} = 0.03$ the maximum value of $\langle Q \rangle = 11.3979 \times 10^{-5}$ at $\chi = 0.95$ and when $\mathrm{Kn} = 0.05$ the maximum value of $\langle Q \rangle = 15.4801 \times 10^{-5}$ at $\chi = 0.9$. From the above discussion, we notice that in absence of the slip effect in this deeply non-Newtonian regime $\langle Q \rangle$ increases with increasing χ. On the other hand, when the slip effect is taken into account we observe that $\langle Q \rangle$ attains a maximum at a certain value of χ and then decreases. Moreover, there is a shift in the maximum value of $\langle Q \rangle$ towards lower values of χ with increasing Kn.

We can observe from Figs. 1, 3 and 4 that when $\mathrm{Kn} = 0.05$ (e.g.), the maximum value of $\langle Q \rangle$ is 2.9734×10^{-5} at $t_m = 0.0$ and $\chi = 0.4$, while the maximum value of $\langle Q \rangle$ is 2.6858×10^{-5} at $\chi = 0.7$ and $t_m = 1000$. Moreover, the maximum value of $\langle Q \rangle$ is 15.4801×10^{-5} at $\chi = 0.9$ and $t_m = 10000$. We can notice from the previous values that the slip boundary condition is affected stronger in the case of a non-Newtonian regime than a Newtonian one. Furthermore, we note

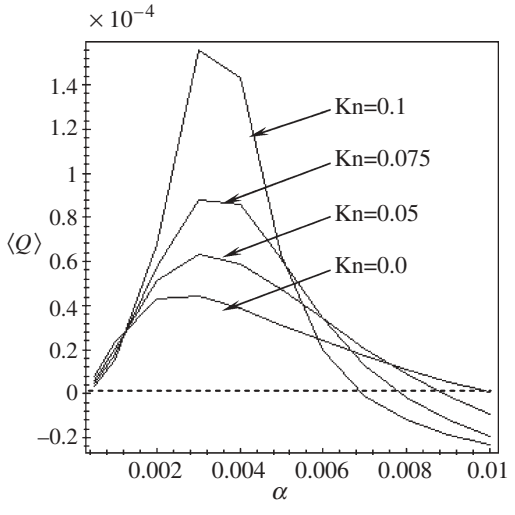

Fig. 5. The dimensionless net flow rate $\langle Q \rangle$ versus α at $\varepsilon = 0.001$, $\mathrm{Re} = 10000.0$, $t_m = 100$ and $\chi = 0.6$

that the slip boundary conditions are weakly affected at incompressible liquid ($\chi = 0.0$), and greatly affected at compressible liquid ($\chi > 0.0$).

In Fig. 5 the dimensionless net flow rate $\langle Q \rangle$ is plotted versus α, which is the tube radius measured in wavelengths, at the following set of parameters: $\varepsilon = 0.001$, $\mathrm{Re} = 10000.0$, $\chi = 0.6$ and $t_m = 100$. We investigate the behavior of the net flow rate $\langle Q \rangle$ on the parameter α at various values of Kn. We observe that for $\alpha < 0.001$ the range of the net flow rate $\langle Q \rangle$ is $0.0367 - 0.0791 \times 10^{-4}$ at various values of Kn ($0.0 \leq \mathrm{Kn} \leq 0.1$). Hence, the net flow rate $\langle Q \rangle$ is nearly independent of Kn for $\alpha < 0.001$. For $0.001 \leq \alpha \leq 0.0065$ we observe that $\langle Q \rangle$ attains a maximum for a certain value of α and this maximum increase with increasing Kn. For $\alpha > 0.0065$ we observe that $\langle Q \rangle$ decreases with increasing Kn. We also note from the figure that at $\mathrm{Kn} = 0.0$ there is no negative value of $\langle Q \rangle$. Furthermore, we observe that $\langle Q \rangle = -0.0113 \times 10^{-4}$ reaches negative values at $\mathrm{Kn} = 0.05$ and $\alpha = 0.009$, while $\langle Q \rangle = -0.0196 \times 10^{-4}$ at $\mathrm{Kn} = 0.075$ and $\alpha = 0.008$, and $\langle Q \rangle = -0.0074 \times 10^{-4}$ at $\mathrm{Kn} = 0.1$ and $\alpha = 0.007$. The negative value of the net flow rate $\langle Q \rangle$ means that we observe backflow. This means that flow occurs in the direction opposite to the direction of propagation of the traveling wave on the tube wall. Moreover, the reverse flow (backflow) occurs easily in the presence of a slip boundary condition and also a non-Newtonian regime. The net flow rate $\langle Q \rangle$ increases in the reverse direction with increasing α.

In Fig. 6 the dimensionless net flow rate $\langle Q \rangle$ is plotted versus α at the following set of parameters: $\varepsilon = 0.001$, $\mathrm{Re} = 10000.0$, $\chi = 0.6$ and $t_m = 1000$. We investigate the behavior of the net flow rate $\langle Q \rangle$ on the parameter α at various values of Kn within the range of $0.0 \leq \alpha \leq 0.01$. We note that at $\mathrm{Kn} = 0.0$ the curve in our Fig. 6 is identical to the curve (dashed – dotted curve with asterisks) in Fig. 2 from [17]. We notice again that there is no back flow at $\mathrm{Kn} = 0.0$, while $\langle Q \rangle = -0.0019 \times 10^{-4}$ at $\alpha = 0.006$ and $\mathrm{Kn} = 0.05$, and $\langle Q \rangle = -0.0818 \times 10^{-4}$ at $\alpha = 0.004$ and $\mathrm{Kn} = 0.1$. If we compare Figs. 5 and 6 we note that when $\mathrm{Kn} = 0.0$ there is no backflow, while at $\mathrm{Kn} = 0.05$ the backflow occurs at $\alpha = 0.009$ when $t_m = 100$, whereas at $\mathrm{Kn} = 0.05$ the backflow occurs at $\alpha = 0.006$ when $t_m = 1000$. Also, at $\mathrm{Kn} = 0.1$ the backflow occurs at $\alpha = 0.007$ when $t_m = 100$, whereas at $\mathrm{Kn} = 0.1$ the backflow occurs at $\alpha = 0.004$ when $t_m = 1000$. From the previous discussion, we note that the backflow easily happened at low values of α, which is the tube radius measured in wavelengths, when t_m, the relaxation time, has a high value (non-Newtonian regime) with high values of Kn.

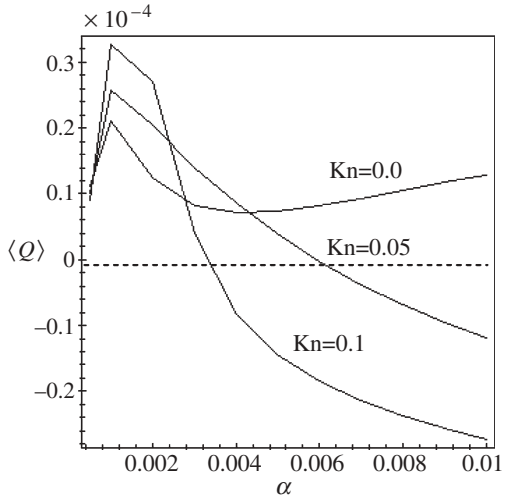

Fig. 6. The dimensionless net flow rate $\langle Q \rangle$ versus α at $\varepsilon = 0.001$, $\mathrm{Re} = 10000.0$, $t_m = 1000$ and $\chi = 0.6$

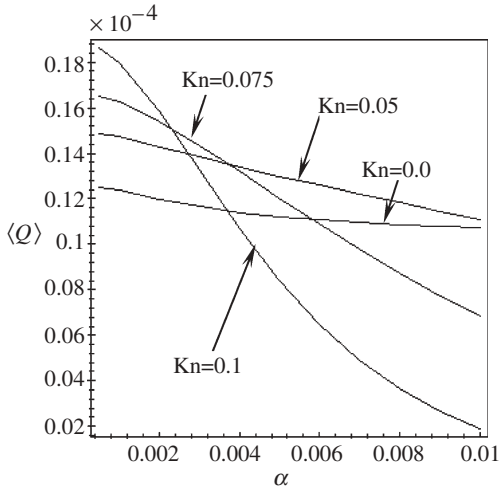

Fig. 7. The dimensionless net flow rate $\langle Q \rangle$ versus α at $\varepsilon = 0.001$, $\mathrm{Re} = 10000.0$, $t_m = 0.0$ and $\chi = 0.0$

To investigate the behavior of an incompressible ($\chi = 0.0$) Newtonian ($t_m = 0.0$) Maxwellian fluid under the slip effect, the dimensionless net flow rate $\langle Q \rangle$ is plotted versus α in Fig. 7 for $\varepsilon = 0.001$, $\mathrm{Re} = 10000.0$, $\chi = 0.0$, $t_m = 0.0$ and $\mathrm{Kn} = (0.0, 0.05, 0.075$ and $0.1)$. We observe that the range of $\langle Q \rangle$ is approximately $1.2507 - 1.0723 \times 10^{-5}$ if $\mathrm{Kn} = 0.0$, $1.4863 - 1.1082 \times 10^{-5}$ if $\mathrm{Kn} = 0.05$, $1.6505 - 0.6820 \times 10^{-5}$ if $\mathrm{Kn} = 0.075$ and $1.8616 - 0.0189 \times 10^{-5}$ if $\mathrm{Kn} = 0.1$ for $0.0005 \leq \alpha \leq 0.01$. Furthermore, at low values of α the net flow $\langle Q \rangle$ increases with increasing Kn and decreases with increasing Kn at high values of α. Moreover, $\langle Q \rangle$ decreases with increasing α and the rate of decreasing of $\langle Q \rangle$ increases with increasing Kn. Also, there is no negative value of $\langle Q \rangle$, which means there is no reversal flow. The behavior of an incompressible ($\chi = 0.0$) non-Newtonian Maxwellian fluid under the slip effect studied in Fig. 8. In this figure the net flow rate $\langle Q \rangle$ is plotted versus α, for $\varepsilon = 0.001$, $\mathrm{Re} = 10000.0$, $\chi = 0.0$, $t_m = 1000.0$ and $\mathrm{Kn} = 0.0$, 0.05 and 0.1. We observe that $\langle Q \rangle$ decreases with increasing α to a certain value of α, then increases with increasing α. Also, we note that (approximately) there are no negative values of $\langle Q \rangle$. Furthermore, we observe that $\langle Q \rangle$ decreases with increasing α and the negative value of $\langle Q \rangle$ for $\mathrm{Kn} = 0.05$ begins at $\alpha = 0.004$ and

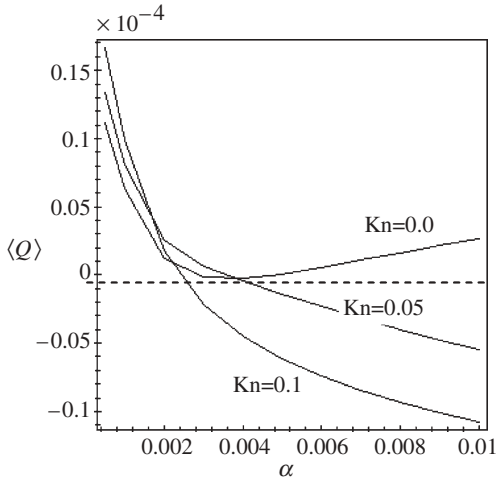

Fig. 8. The dimensionless net flow rate $\langle Q \rangle$ versus α at $\varepsilon = 0.001$, $\mathrm{Re} = 10000.0$, $t_m = 1000$ and $\chi = 0.0$

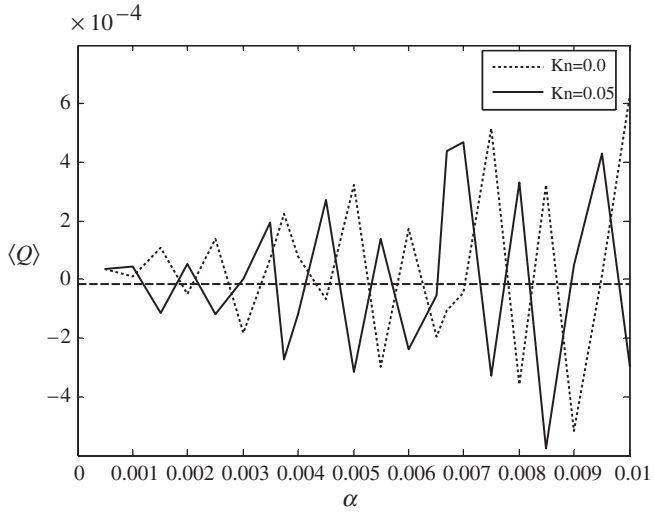

Fig. 9. The dimensionless net flow rate $\langle Q \rangle$ versus α at $\varepsilon = 0.001$, $\mathrm{Re} = 10000.0$, $t_m = 10000$ and $\chi = 0.6$

equals -0.0489×10^{-5}, while the negative value of $\langle Q \rangle$ for $\mathrm{Kn} = 0.1$ begins at $\alpha = 0.003$ and equals -0.2146×10^{-5} then increases in reversal direction with increasing α to value equals -1.0778×10^{-5} at $\alpha = 0.01$.

In Fig. 9 the net flow rate $\langle Q \rangle$ is plotted versus α for the following set of parameters: $\varepsilon = 0.001$, $\mathrm{Re} = 10000.0$, $\chi = 0.6$ and $t_m = 10000$ (deeply non-Newtonian regime) and various values of Kn within the range of $0.0 \leq \alpha \leq 0.01$. We note that at $\mathrm{Kn} = 0.0$ the curve in our Fig. 6 is the same as the curve in Fig. 2 from [17]. We note from this figure that in this deeply non-Newtonian regime $\langle Q \rangle$ becomes highly oscillatory, but what is unusual again is that we observe the negative flow rates for certain values of α. Oscillatory behavior (appearance of numerous maxima in the behavior of a physical value) in the deeply non-Newtonian regime is not new [17]. We notice that the oscillations at $\mathrm{Kn} = 0.0$ are approximately the same as at $\mathrm{Kn} = 0.05$ but there is a shift in the value of $\alpha \cong 0.0005$. For example, $\langle Q \rangle = 0.0003 \times 10^{-4}$ when $\mathrm{Kn} = 0.0$ and $\alpha = 0.0085$, whereas $\langle Q \rangle = 0.0003 \times 10^{-4}$ when $\mathrm{Kn} = 0.05$ and $\alpha = 0.008$. We note the same value of $\langle Q \rangle$, approximately, at $\mathrm{Kn} = 0.0$ and $\mathrm{Kn} = 0.05$ but there is shifting of the value of α.

5 Conclusions

In real systems there is always a certain amount of slip, which, however, is hard to detect experimentally because of the required space resolution. No-slip boundary conditions are a convenient idealization of the behavior of viscous fluids near walls. The boundary conditions relevant to flowing fluids are very important in predicting fluid flows in many applications. In this paper, we investigated the dynamics of fluid flow in an axisymmetric cylindrical tube (pore) induced by a wave traveling on its wall (boundary). This problem has numerous applications in various branches of science, including stimulation of fluid flow in porous media under the effect of elastic waves and studies of blood flow dynamics in living creatures. We investigate phenomena brought about into the classic peristaltic mechanism by the inclusion of slip effects based on the model of a Newtonian and non-Newtonian Maxwellian fluid in an axisymmetric cylindrical tube (pore). The viscosity as well as the compressibility of the liquid is taken into

account. We have found that the compressibility number χ has a significant influence on the net flow rate as shown in [1] and [17], and the Knudsen number Kn plays a more significant role in the net flow of a compressible liquid than of an incompressible one. Also we can note that $\langle Q \rangle$ is nearly independent of Kn for the values of $\alpha < 0.001$. We notice that at $\chi = 0.0$ and small values of χ the net flow rate $\langle Q \rangle$ increases with increasing Kn, thereby establishing the fact that the slip causes enhanced flow of incompressible liquid. This is physically acceptable. On the other hand, we notice that the net flow rate $\langle Q \rangle$ decreases with increasing Kn at high values of the compressibility number χ. Moreover, the reversal flow occurs at high values of the compressibility number and high values of Kn where $\langle Q \rangle$ becomes negative, i.e., we observe backflow. Thus, the reversal flow could occur easily in the case of compressible liquid than the incompressible one at high values of the Knudsen number.

In absence of the slip effect in the deeply non-Newtonian regime, the net flow rate $\langle Q \rangle$ increases with increasing compressibility parameter χ. On the other hand, when the slip effects are taken into account we observe that $\langle Q \rangle$ attains a maximum at a certain value of χ and then decreases. Moreover, there is a shift in the maximum value of $\langle Q \rangle$ towards lower values of χ with increasing Kn. Furthermore, the slip boundary condition is affected stronger in the case of the non-Newtonian regime than the Newtonian one. The reverse flow (backflow) occurs easily in presence of a slip boundary condition and in the non-Newtonian regime. Also, the backflow easily happened at low values of α, which is the tube radius measured in wavelengths, when t_m, the relaxation time, has a high value (non-Newtonian regime) with high values of Kn. In the deeply non-Newtonian regime $\langle Q \rangle$ becomes high oscillatory, but what is unusual again is that we observe the negative flow rates for certain values of α. Oscillatory behavior (the appearance of numerous maxima in the behavior of a physical value) in the deeply non-Newtonian regime is not new [17].

Acknowledgements

The authors would like to deeply express their thanks to the referees for valuable comments.

References

[1] Aarts, A. C. T., Ooms, G.: Net flow of compressible viscous liquids induced by traveling waves in porous media. J. Engng. Math. **34**, 435–450 (1998).
[2] Antanovskii, L. K., Ramkisson, H.: Long wave peristaltic transport of a compressible viscous liquid in a finite pipe subject to a time-dependent pressure drop. Fluid Dyn. Res. **19**, 115–123 (1997).
[3] Jabbarzadeh, A., Atkinson, J. D., Tanner, R. I.: Effect of the wall roughness on slip and rheological properties of hexadecane in molecular dynamics simulation of Couette shear flow between two sinusoidal walls. Phys. Rev. E **61**(1), 690–699 (2000).
[4] Kwang, W., Chu, H., Fang, J.: Peristaltic transport in a slip flow. Euro. Phys. J. B **16**, 543–547 (2000).
[5] Georgiou, G. C., Crochet, M. J.: Compressible viscous flow in slits with slip at the wall. J. Rheol. **38**(3), 639–654 (1994).
[6] Lu, F., Lee, H. P., Lim, S. P.: Mechanical description of interfacial slips for quartz crystal micro balances with viscoelastic liquid loading. Smart Mater. Struct. **12**, 881–898 (2003).
[7] Castrejon-Pita, J. R., del Rio, J. A., Castrejon-Pita, A. A., Huelsz, G.: Experimental observation of dramatic differences in the dynamic response of Newtonian and Maxwellian fluids. Phys. Rev. E **68**, 046301 (2003).

[8] Torralba, M., Castrejon-Pita, A. A., Castrejon-Pita, J. R., Huelsz, G., del Rio, J. A., Ortin, J.: Measurements of the bulk and interfacial velocity profiles in oscillating Newtonian and Maxwellian fluids. Phys. Rev. E **72**, 016308 (2005).
[9] Roa, I. J., Rajagapol, K. R.: The effect of slip boundary conditions on the flow of fluids in a channel. Acta Mech. **135**, 113–126 (1999).
[10] Larrode, F. E., Housiadas, C., Drossinos, Y.: Slip-flow heat transfer in circular tubes. Int. J. Heat Mass Transfer **43**, 2669–2680 (2000).
[11] Chu, W.: Stokes slip flow between corrugated walls. ZAMP **47**, 591–598 (1996).
[12] Chu, K.-H. W.: Small-Knudsen-number flow in a corrugated tube. Meccanica **34**, 133–137 (1999).
[13] Kogan, M. N.: Rarefied gas dynamics. New York: Plenum Press 1969.
[14] Vasudeviah, A., Balamurugan, K.: Stokes slip flow in a corrugated pipe. Int. J. Engng. Sci. **37**, 1629–1641 (1999).
[15] Zhu, Y., Granick, S.: Limits of the hydrodynamic no-slip boundary condition. Phys. Rev. Lett. **88**(10), 106102 (2002).
[16] Yin, F., Fung, Y. C.: Peristaltic waves in circular cylindrical tubes. J. App. Mech. **36**, 579–587 (1969).
[17] Tsiklauri, D., Beresnev, I.: Non-Newtonian effects in the peristaltic flow of a Maxwell fluid. Phys. Rev. E **64**, 036303 (2001).
[18] Del Rio, J. A., De Haro, M. L., Whitaker, S.: Enhancement in the dynamic response of a viscoelastic fluid flowing in a tube. Phys. Rev. E **58**, 6323–6327 (1998).
[19] Anderson, J. D.: Modern compressible flow with historical perspective. McGraw-Hill Publishing Co. 1990.
[20] Wang, C. Y.: Stagnation flows with slip: exact solutions of the Navier-Stokes Equations. ZAMP **54**, 184–189 (2003).
[21] Beavers, G. S., Joseph, D. D.: Boundary conditions at a naturally permeable wall. J. Fluid Mech. **30**, 197–207 (1967).
[22] Nayfeh, A. H.: Perturbation methods. John Wiley & Sons 1973.
[23] Takabatake, S., Ayukawa, K., Mori, A.: Peristaltic pumping in circular cylindrical tubes: a numerical study of fluid transport and its efficiency. J. Fluid Mech. **193**, 267–283 (1988).

Authors' addresses: E. F. El-Shehawy and N. T. El-Dabe, Department of Mathematics, Faculty of Education, Ain Shams University, Heliopolis, Cairo, Egypt; I. M. El-Desoky, Department of Basic Engineering Sciences, Faculty of Engineering, Menofia University, Shebin El-Kom, Menofia, Egypt (E-mail: eldesokyi@yahoo.com)